An improved passive scalar model for hydrogen hazardous ignition prediction

Marc Le Boursicaud, Song Zhao, Jean-Louis Consalvi, Pierre Boivin

An improved passive scalar model for hydrogen hazardous ignition prediction

Marc Le Boursicaud[a,*], Song Zhao[a], Jean-Louis Consalvi[b], Pierre Boivin[a]

[a] *Aix Marseille Univ, CNRS, Centrale Marseille, M2P2, Marseille, France*
[b] *Aix Marseille Univ, CNRS, IUSTI, Marseille, France*

Abstract

With an increasing interest in hydrogen as an alternative fuel for transportation, there is a need to develop tools for the prediction of ignition events. A cost-effective passive scalar formulation has been recently developed to predict hydrogen auto-ignition. A single scalar advection-diffusion-reaction equation is used to reproduce the chain-branched ignition process, where the scalar represents the radical pool responsible of ignition (H, O, OH, HO_2, H_2O_2). The scalar reaction rate is analytically deduced from the Jacobian matrix associated to hydrogen ignition chemistry. This method was found to reproduce with good accuracy the ignition delays obtained by detailed chemistry for temperature where the branching is the leading process. For temperature close or below the crossover temperature, where other phenomenon such as the thermal runaway are important, the scalar approach fails to predict correctly ignition events. Thus, an extension of the scalar source term formulation is proposed to extend its validity over the entire temperature range. In addition, a simple way to approximate the diffusion properties of the scalar is introduced: the radical pool composition may vary drastically, with molecules having very different diffusion properties (e.g. H and HO_2). The complete modified framework is presented and its capability is assessed in canonical scenarios and more complex simulations relevant to hydrogen safety.

Keywords: Auto-ignition, Hydrogen, Hydrogen safety, reduced chemistry

*Corresponding author.
Email address: marc.leboursicaud@gmail.com (Marc Le Boursicaud)

1. Introduction

Hydrogen is now being seriously considered as an energy carrier for a wide range of applications. For instance, Airbus ZERO-e program aims at flying a 100% H_2-fueled aircraft by 2035, which opens many H_2 safety questions. Hydrogen explosion limits, described in the classical Lewis & von Elbe textbook [1] are well understood, and analytical expressions for ignition delays are available throughout the literature (see, e.g. [2]).

In predicting hazardous ignition, two main methodologies are available in the literature. The first one consists in analytically deriving ignition in canonical configurations: ignition in mixing layers [3], thermal-induced (hot-wall) ignition [4, 5], shock-induced ignition [6, 7], minimal energy required for kernel ignition [8, 9], critical radius for hot-jet ignition [10, 11], etc. The second method consists in simulating the configuration considered using a reactive Navier-Stokes solver, using a H_2 chemical description able to accurately reproduce ignition delays. Given the small characteristic chemical time scales associated with H_2 chemistry, such simulations are expensive because they require a large number of time steps.

The present study builds upon the observation that characteristic chemical time scales associated to ignition are typically much larger than the chemical time scales associated to flames [12]. For safety studies, where the main question is whether there is an ignition risk, it is therefore interesting to build reduced chemical descriptions that accurately reproduce ignition, but that do not include whatsoever the short time scales involved in H_2 flames.

In our previous work [13], we introduced a passive scalar η (with the dimension of a mass fraction), intended to represent all intermediate species relevant for hydrogen ignition. The evolution of η is governed by a classical advection-diffusion-reaction equation:

$$\frac{\partial \rho \eta}{\partial t} + \frac{\partial \rho u_\alpha \eta}{\partial x_\alpha} = \frac{\partial}{\partial x_\alpha}\left(\rho D_\eta \frac{W_\eta}{W}\frac{\partial}{\partial x_\alpha}\left(\frac{W}{W_\eta}\eta\right)\right) + \dot{\omega}_\eta \tag{1}$$

with a source term $\dot{\omega}_\eta$, and diffusion coefficient D_η. Through careful derivation of these two terms, the scalar model was shown to accurately predict the lift-off of the H_2-air lifted jet flame experimentally investigated by Cabra *et al.* [14]. This was achieved for a fraction of the cost of the full reactive simulation – also presented in [13] – because hydrogen ignition has a characteristic time scale significantly larger than the flame characteristic time scale, and because intermediate species become unnecessary, with only

H_2 and O_2 being required in the computation. Nonetheless, the study benefited from the knowledge that ignition would occur above crossover, where ignition overwhelmingly corresponds to an H-atom branch-chained explosion. Accordingly, the η properties were chosen to match those of H-atom.

The objective of the present paper is to extend and improve the formulation by modifying $\dot{\omega}_\eta$ and D_η, so it can predict ignition hazards for all temperatures, including close or below crossover. The article is organized as follows. Section 2 introduces the necessary notations, and recalls the derivation of $\dot{\omega}_\eta$ used in [13]. Section 3 extends the formulation, to take into account the thermal runaway responsible for the third explosion limit and the ignition at low temperatures or high pressures. Section 4 investigates the effect of the radical pool diffusion properties through D_η. The article closes with conclusions and perspectives.

2. The ignition scalar model

2.1. Minimal hydrogen ignition description

The study starts by identifying the main steps responsible for H_2 ignition under a wide range of conditions. In light of previous analytical studies [15–17], our starting point is the skeletal mechanism presented in Tab. 1, which also provides the corresponding Arrhenius rates, extracted from the up-to-date San Diego mechanism [18]. The 8 steps include the classical branching (1-3), termination (4), and initiation steps (5) which have long been identified as responsible for high-temperature ignition [19, 20]. The additional steps (6-8) have been found important in the description of low-temperature ignition events [15, 19], also corresponding to the chemistry underlying the third-explosion limit of H_2-air systems [21].

This choice of skeletal description is validated in Fig. 1, which compares ignition delays of stoichiometric H_2-air mixtures for a wide range of pressure/temperature conditions, as obtained with the detailed San Diego mechanism [18] and with the 8-step mechanism. An excellent agreement is obtained in all presented cases. Although it is not shown here, a similar agreement is obtained when varying the equivalence ratio and dilution.

Throughout the paper, use is made of the classical crossover definition for hydrogen ignition [2]. It is defined as the crossover temperature T_c for which the rate of reaction $O_2 + H \rightarrow OH + O$ is half that of the third-body reaction $H + O_2 + M \rightarrow HO_2 + M$. Introducing the crossover variable α as

$$\alpha = \frac{2k_1}{k_4 C_M}, \tag{2}$$

Table 1: Chemical reactions responsible for hydrogen ignition and corresponding rates in Arrhenius form $k = AT^n \exp(-E_a/RT)$. Rates numerical values are extracted from the up-to-date San Diego mechanism [18].

	Reaction		A^a	n^a	E_a^a
1	$H+O_2 \rightarrow OH+O$		$3.52\ 10^{16}$	-0.7	71.42
2	$H_2+O \rightarrow OH+H$		$5.06\ 10^{4}$	2.67	26.32
3	$H_2+OH \rightarrow H_2O+H$		$1.17\ 10^{9}$	1.3	15.17
4	$H+O_2+M \rightarrow HO_2+M^b$	k_0	$5.75\ 10^{19}$	-1.4	0.0
		k_∞	$4.65\ 10^{12}$	0.44	0.0
5	$H_2+O_2 \rightarrow HO_2+H$		$2.93\ 10^{12}$	0.356	232.21
6[c]	$2HO_2 \rightarrow H_2O_2+O_2$		$1.03\ 10^{14}$	0.0	46.22
			$1.94\ 10^{11}$	0.0	-5,89
7	$HO_2+H_2 \rightarrow H_2O_2+H$		$7.80\ 10^{10}$	0.61	100.14
8	$H_2O_2+M \rightarrow 2OH+M^d$	k_0	$7.60\ 10^{30}$	-4.20	213.71
		k_∞	$2.63\ 10^{19}$	-1.27	214.74

[a]Units are mol, s, cm^3, kJ, and K.

[b]Chaperon efficiencies are 2.5 for H_2, 16.0 for H_2O, 0.7 for Ar and He and 1.0 for all other species; Troe falloff with $F_c = 0.5$

[c]Bi-Arrhenius (the sum of the two constants).

[d]Chaperon efficiencies are 2.0 for H_2, 6.0 for H_2O, 0.4 for Ar and He, and 1.0 for all other species; $F_c = 0.265 \exp(-T/94\text{K}) + 0.735 \exp(-T/1756\text{K}) + \exp(-5182\text{K}/T)$

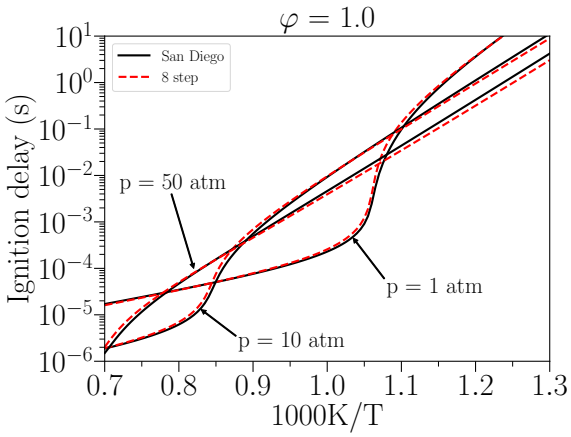

Figure 1: Comparison of ignition delays of a stoichiometric hydrogen-air mixture, obtained by numerical integration for the detailed San Diego mechanism (solid black lines) and the 8-step skeletal mechanism (red dashed lines).

we then have $\alpha > 1$ for temperatures above crossover, where H, O, and OH are the main chain-branching carriers; while HO_2 and H_2O_2 are dominant at low temperature ($\alpha < 1$, below the crossover temperature T_c).

2.2. Recap and notations

Hydrogen chemistry includes 5 intermediate species H, O, OH, HO_2, and H_2O_2, but their proportion varies strongly depending on the local conditions. Their rate of production may be written as

$$\frac{\mathrm{d}\bar{C}}{\mathrm{d}t} = \mathbf{A}\bar{C} + \bar{\epsilon}, \tag{3}$$

where $\bar{C}$ is the radical-pool molar concentration vector:

$$\bar{C} = \begin{bmatrix} C_{\mathrm{H}} & C_{\mathrm{O}} & C_{\mathrm{OH}} & C_{\mathrm{HO_2}} & C_{\mathrm{H_2O_2}} \end{bmatrix}^T, \tag{4}$$

$\mathbf{A}$ is the chemical Jacobian matrix, and $\bar{\epsilon}$ is an initial rate vector. Neglecting step 6, they read

$$\mathbf{A} = \begin{bmatrix} -(l_1+l_4) & l_2 & l_3 & l_7 & 0 \\ l_1 & -l_2 & 0 & 0 & 0 \\ l_1 & l_2 & -l_3 & 0 & 2l_8 \\ l_4 & 0 & 0 & -l_7 & 0 \\ 0 & 0 & 0 & l_7 & -l_8 \end{bmatrix}, \quad \text{and} \quad \bar{\epsilon} = \begin{bmatrix} \omega_5 \\ 0 \\ 0 \\ \omega_5 \\ 0 \end{bmatrix}. \tag{5}$$

Above, ω_k is the reaction rate of the k^{th} reaction (e.g. $\omega_1 = k_1 C_{\mathrm{O_2}} C_{\mathrm{H}}$) as given in Tab. 1, and l_k is the corresponding inverse characteristic time (e.g. $l_1 = k_1 C_{\mathrm{O_2}}$), which only depend on temperature, pressure, and major species (H_2, O_2, and diluent). Note that Eq. (3) can be analytically solved for a homogeneous system, by assuming temperature and main reactants (H_2, O_2) are constant throughout the ignition process (i.e. $\mathbf{A}$, Eq. 5, is a constant). These approximations provided useful expressions for ignition delays [16, 17, 19, 20], but will not be necessary hereafter.

System (3), through diagonalization of $\mathbf{A}$ (5), can be rewritten as

$$\mathbf{P}^{-1}\frac{\mathrm{d}\bar{C}}{\mathrm{d}t} = \mathbf{D}\mathbf{P}^{-1}\bar{C} + \mathbf{P}^{-1}\bar{\epsilon}, \tag{6}$$

With $\mathbf{D}$ and $\mathbf{P}^{-1}$ the diagonal and the left eigenvectors matrix such that $\mathbf{A} = \mathbf{P}\mathbf{D}\mathbf{P}^{-1}$. Upon noting that the $\mathbf{A}$'s largest eigenvalue λ quickly dominates the ignition history [16] (the other eigenvalues being rapidly negligible

or simply evanescent modes), the only equation of interest among the five decoupled equations in Eq. (6) can be expressed as:

$$\bar{V}^L \frac{\mathrm{d}\bar{C}}{\mathrm{d}t} = \lambda \bar{V}^L \bar{C} + \bar{V}^L \bar{\epsilon}, \tag{7}$$

with $\bar{V}^L$ the left eigenvector associated to λ (the row of $\mathbf{P}^{-1}$ corresponding to λ). We then introduce a scalar C_η (with molar concentration units) following the same equation evolution as the scalar $\bar{V}^L \bar{C}$ such that $\bar{C} \approx \bar{V}^R C_\eta$:

$$\frac{\mathrm{d}C_\eta}{\mathrm{d}t} = \lambda C_\eta + \epsilon_\eta, \tag{8}$$

with $\epsilon_\eta = \bar{V}^L \bar{\epsilon} = \left(V^L_{\mathrm{H}} + V^L_{\mathrm{HO_2}}\right) \omega_5$, where V^L_{H} and $V^L_{\mathrm{HO_2}}$ are the first and fourth elements of $\bar{V}^L$. Since the eigenvector associated with eigenvalue λ has dimension one, a relationship between C_η and $\bar{C}$ is needed, for which details are included in Appendix A.

For the remainder of the present study, $\epsilon_\eta = \omega_5$ have been retained for simplicity (no need to compute the full $\mathbf{P}$ matrix), resulting in $C_\eta \approx C_{\mathrm{H}}$ at high temperature and $C_\eta \approx C_{\mathrm{HO_2}}$ below the cross-over temperature. As will be discussed later, those properties will be useful in the new framework.

The ignition scalar η [mass fraction] in Eq. (1) is then related to C_η [molar concentration] through:

$$C_\eta = \rho \frac{\eta}{W_\eta}, \tag{9}$$

with W_η the molecular weight of species η. From the above, one finally obtains the scalar production rate $\dot{\omega}_\eta$ missing in (1):

$$\dot{\omega}_\eta = (\lambda C_\eta + \epsilon_\eta)\, W_\eta. \tag{10}$$

Hereafter, we assume $W_\eta = W_{\mathrm{H}}$, as in [13]. This choice has no impact on the results, as detailed in Appendix B.

2.3. Limitations of the initial scalar model

The study by Taileb et al. [13] benefited from prior knowledge that the configuration studied was igniting above crossover ($\alpha > 1$), and in a relatively rich region, where the radical pool overwhelmingly consists of H-atom [16], so $\eta \approx Y_{\mathrm{H}}$, or $C_\eta \approx C_{\mathrm{H}}$.

Figure 2.a represents the evolution of C_η compared with that of C_{H} as well as the normalized temperature $\Theta = (T - T_0)/(T^{8\mathrm{step}}_{max} - T_0)$, in an isobaric

homogeneous reactor, initially filled with a stoichiometric H_2-air mixture at p=1 atm and T_0=1100 K, well above crossover. C_η results from the sole

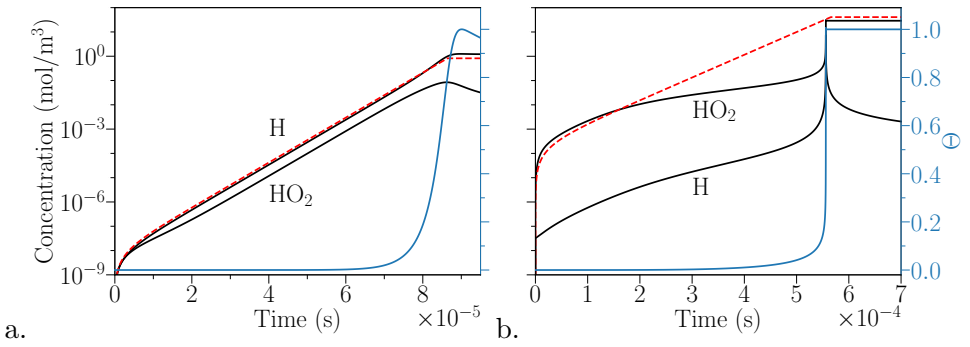

Figure 2: Normalized temperature (blue line, right axis), H and HO_2 concentrations (black lines, left axis) as functions of time, during isobaric homogeneous ignition processes from numerical integration with the 8-step skeletal chemistry for φ=1.0, with p=1 atm, T_0=1100 K ($> T_c$, left) and p=50 atm, T_0=1100 K ($< T_c$, right). Through the integration of Eq.(8), C_η is also presented, until it reaches the limitant reactant concentration $C_\eta = \min(C_{H_2}, C_{O_2}/2)$ (red dashed, left axis).

integration of Eq. (8) (having discarded convection and diffusion). It is clear that C_η and C_H follow the exact same trend, even though the heat release is neglected, and that $C_\eta = \min(C_{H_2}, C_{O_2}/2)$ is an adequate condition to indicate ignition (materialized by the C_η curve horizontal level) [22] .

Let us repeat now the exercise at p=50 atm, for the same temperature T_0=1100 K (below crossover) in Fig. 2.b, and assuming now $C_\eta = C_{HO_2}$, the main chain-carrier in this domain [16]. It is now clear that C_η follows closely the evolution of C_{HO_2}, but only in the very early stage of the ignition process. This behaviour calls for the new formulation presented hereafter.

3. An improved scalar model

The process leading to ignition for temperature below the cross-over temperature is in appearance simpler than the one at high temperature because the radicals H, O and OH, can be assumed in a quasi-steady-state [15]. However, the chemical pathway followed by HO_2 and H_2O_2 evidences the importance of the non-linear branching step 6 that slows down the chain-branching leaving place to a thermal runaway [19]. Improving the description of the ignition close to and below crossover ($\alpha \lesssim 1$) then requires (i) to include step 6 in the rate, and (ii) take into account the thermal runaway,

neglected here since η production does not yield any heat release. These two points are successively discussed in the next two Sections.

3.1. The non-linearity of step 6

As previously mentioned, reaction 6 cannot be neglected in the low-temperature regime, leading to the new concentration evolution equation:

$$\frac{\mathrm{d}\bar{C}}{\mathrm{d}t} = \mathbf{A}\bar{C} + \bar{B}\left(\bar{C}\right) + \bar{\epsilon} \tag{11}$$

with $\bar{B}$ the vector containing the non-linear branching reactions:

$$\bar{B} = \begin{bmatrix} 0 & 0 & 0 & -2k_6 C_{\mathrm{HO}_2}^2 & k_6 C_{\mathrm{HO}_2}^2 \end{bmatrix}^T. \tag{12}$$

Following the study by Liang *et al.* [23] on the role of this non-linear step in defining the H_2 explosion limits, the system is considered to have a linear form with respect to the concentration vector by linearizing $\bar{B}$ and including it in the Jacobian :

$$\mathbf{J} = \mathbf{A} + \frac{\mathrm{d}\bar{\mathrm{B}}}{\mathrm{d}\bar{\mathrm{C}}} = \begin{bmatrix} -(l_1+l_4) & l_2 & l_3 & l_7 & 0 \\ l_1 & -l_2 & 0 & 0 & 0 \\ l_1 & l_2 & -l_3 & 0 & 2l_8 \\ l_4 & 0 & 0 & -l_7-4l_6 & 0 \\ 0 & 0 & 0 & l_7+2l_6 & -l_8 \end{bmatrix}, \tag{13}$$

with $l_6 = k_6 C_{\mathrm{HO}_2}$. Linearization of the system leads to a new Jacobian $\mathbf{J}$ largest eigenvalue $\lambda^{(l_6)}$. Unlike λ, $\lambda^{(l_6)}$ now depends on the HO_2 concentration via l_6. This in practice does not lead to any additional difficulty since the model in Taileb *et al.* [13] already required a local $\dot{\omega}_\eta$ computation at every time step, which becomes:

$$\dot{\omega}_\eta = \left[\lambda^{(l_6)} C_\eta + \epsilon_\eta\right] W_\eta. \tag{14}$$

Figure 3.a represents the same ignition test as in Fig. 2.b by solving now Eq. (11) instead of Eq. (3). It appears clearly that the time-evolution of the scalar now reproduces very well that of C_{HO_2}, until the very final thermal runaway.

Finally, an approximation of l_6 is required to evaluate the Jacobian $\mathbf{J}$, since C_{HO_2} is a priori not known. Below crossover, $C_\eta \approx C_{\mathrm{HO}_2}$, as evidenced in Appendix A. Above crossover, $C_{\mathrm{HO}_2} \ll C_\eta$, and step 6 can be neglected,

as was shown in numerous analytical studies [16, 19, 20]. In light of these arguments, l_6 can then be approximated as $k_6 C^*_{\mathrm{HO}_2}$ using

$$C^*_{\mathrm{HO}_2} = \frac{C_\eta}{1+\alpha}, \tag{15}$$

where α is the crossover variable (2). Note that alternative forms for (15) are possible, as long as its limits below and above crossover satisfy respectively $\lim_{\alpha\to 0} C^*_{\mathrm{HO}_2} = C_\eta$ and $\lim_{\alpha\to\infty} C^*_{\mathrm{HO}_2} = 0$.

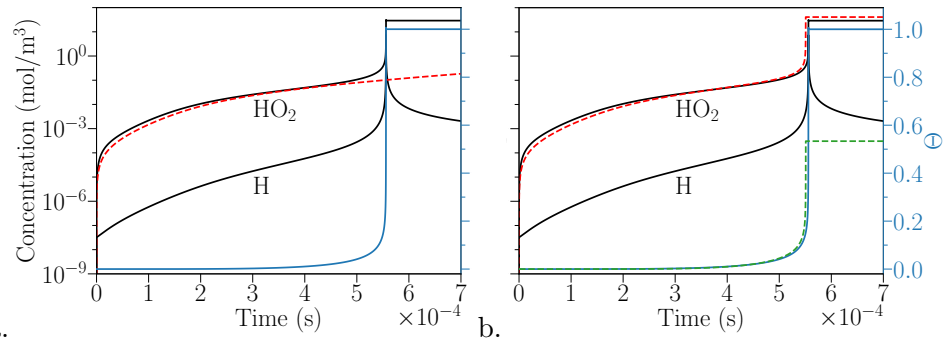

Figure 3: Normalized temperature (blue line, right axis), H and HO_2 concentrations (black lines, left axis) as functions of time, during isobaric homogeneous ignition processes from numerical integration with the 8-step skeletal chemistry for φ=1.0, with T_0=1100 K $< T_c$ and p=50 atm. The integration of C_η is also presented (red dashed, left axis) using the step 6 linearization of Eq. 14 (left), or step 6 linearization and thermal runaway correction of Eq. 34 (right) with the corresponding Θ (green dashed curve) computed using the $\theta - C_\eta$ relationships of Eq. 33.

3.2. Analytical solution for the eigenvalue of interest

As shown previously by Boivin et al. [16, 24], it is possible to obtain accurate analytical predictions for the largest eigenvalue λ. Hereafter, it is proposed to slightly improve the expressions derived in [16]. The study of the Jacobian above crossover corresponding to the upper left 3×3 submatrix $\mathbf{J}_+ = \mathbf{A}_+$, initially proposed in [24] is kept unchanged:

$$\mathbf{J}_+ = \begin{bmatrix} -(l_1+l_4) & l_2 & l_3 \\ l_1 & -l_2 & 0 \\ l_1 & l_2 & -l_3 \end{bmatrix}, \tag{16}$$

the largest eigenvalue λ_+ of which is obtained by neglecting the cubic term of its characteristic polynomial [24], giving

$$\lambda^+ = \frac{\sqrt{a_1^2 - 4a_0a_2} - a_1}{2a_2}, \tag{17}$$

with

$$\begin{cases} a_0 &= (l_4 - 2l_1)l_2l_3 \\ a_1 &= l_2l_3 + l_4(l_2 + l_3) \\ a_2 &= l_1 + l_2 + l_3 + l_4. \end{cases} \tag{18}$$

The largest eigenvalue λ of the 5×5 system can be approximated from an intermediate system obtained by assuming O and OH steady states, valid around and below the cross-over:

$$\frac{\mathrm{d}\bar{C}_t}{\mathrm{d}t} = \mathbf{J_t}\bar{C}_t + \bar{\epsilon}_t, \tag{19}$$

with $\bar{C}_t = [C_{\mathrm{H}}, C_{\mathrm{HO_2}}, C_{\mathrm{H_2O_2}}]^T$, $\bar{\epsilon}_t = [\omega_5, \omega_5, 0]^T$ and

$$\mathbf{J_t} = \begin{bmatrix} 2l_1 - l_4 & l_7 & 2l_8 \\ l_4 & -l_7 - 4l_6 & 0 \\ 0 & l_7 + 2l_6 & -l_8 \end{bmatrix}. \tag{20}$$

The largest eigenvalue matches the one of the 5×5 systems in the low-temperature regime, where O and OH are in steady state [15]. However, it differs in the high-temperature range, where the rate should be λ^+ instead of $2l_1 - l_4$ [24]. By applying the methods develop in [16], the submatrix $\mathbf{J_t}$ can be corrected by multiplying the first line (H-atom production rate) by $\Lambda^+ = \lambda^+/(2l_1 - l_4)$, yielding a new 3×3 matrix $\mathbf{J}_\pm$:

$$\mathbf{J}_\pm = \begin{bmatrix} (2l_1 - l_4)\Lambda_+ & l_7\Lambda_+ & 2l_8\Lambda_+ \\ l_4 & -l_7 - 4l_6 & 0 \\ 0 & l_7 + 2l_6 & -l_8 \end{bmatrix}, \qquad \Lambda^+ = \frac{\lambda^+}{2l_1 - l_4} \tag{21}$$

which now has a maximum eigenvalue $\lambda_\pm$ close to that of the full 5×5 system, solution of the cubic characteristic polynomial

$$\lambda_\pm^3 + b_2\lambda_\pm^2 + b_1\lambda_\pm + b_0 = 0, \tag{22}$$

where

$$\begin{cases} b_0 &= -4l_4l_6l_8\Lambda_+ - 3l_4l_7l_8\Lambda_+ - 4l_6l_8\lambda_+ - l_7l_8\lambda_+ \\ b_1 &= -l_4l_7\Lambda_+ + 4l_6l_8 - 4l_6\lambda_+ + l_7l_8 - l_7\lambda_+ - l_8\lambda_+ \\ b_2 &= 4l_6 + l_7 + l_8 - \lambda_+. \end{cases} \tag{23}$$

Unlike in [22], the cubic term $\lambda_{\pm}^3$ is non-negligible in (22), but the Cardan method still provides an analytical solution for $\lambda_{\pm}$, given in Appendix C.

Figure 4 compares for a wide range of conditions the exact solution for the largest eigenvalue of the 5×5 system $\mathbf{J}$ (obtained numerically) and that obtained analytically from the reduced 3×3 system (C.6). The curves for the exact and analytical eigenvalues are indiscernible with relative errors below 10^{-3}. From now on, only the analytical approximation given (C.6) will be used.

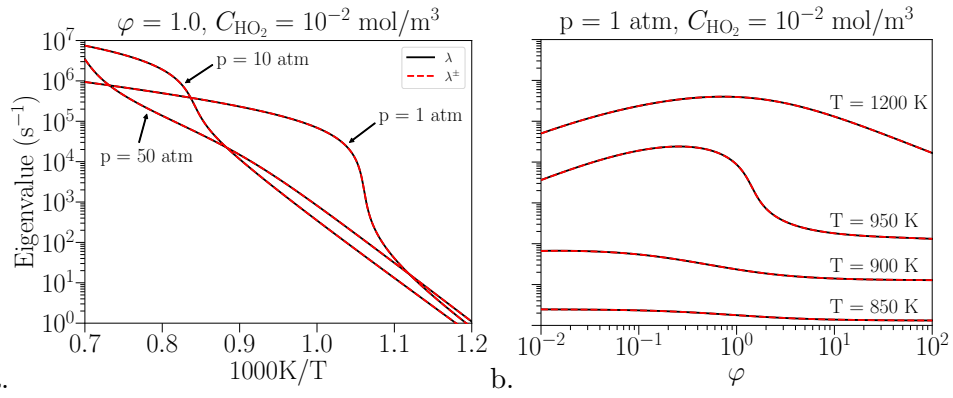

Figure 4: Exact (black line) and analytical (red dashed) eigenvalues λ of the new Jacobian (13) for a stoichiometric H_2-Air mixture with an imposed HO_2 concentration of 10^{-2} mol/m^3 for the coefficient l_6. The analytical eigenvalue $\lambda_{\pm}$ is computed using the method developed in Appendix C applied to the matrix (21).

3.3. Low temperature thermal-runaway

The modifications made in the two previous subsections allow to accurately and efficiently predict the evolution of HO_2 prior to the release of heat for the low temperature regime. In this regime, the thermal-runaway phenomenon, mainly due to the creation of H_2O, has also to be included in the model to predict ignition [15, 21]. In the 8 step mechanism, H_2O is only produced through reaction 3:

$$\frac{\mathrm{d}C_{H_2O}}{\mathrm{d}t} = l_3 C_{OH}. \tag{24}$$

In order to find a relationship between C_{OH} and C_{HO_2} to inject in (24), we first need to assume H and O in quasi-steady-state, which gives the equation:

$$-l_4 C_H + l_3 C_{OH} + l_7 C_{HO_2} = 0. \tag{25}$$

In addition, asymptotic analysis of the thermal runaway below crossover [15, 21] showed that C_{HO_2} may be assumed to be in a steady state, leading to:

$$l_4 C_{\mathrm{H}} - l_7 C_{\mathrm{HO}_2} - 2k_6 C_{\mathrm{HO}_2}^2 = 0. \tag{26}$$

By adding (25) and (26) we obtain the relationship:

$$l_3 C_{\mathrm{OH}} = 2k_6 C_{\mathrm{HO}_2}^2. \tag{27}$$

Making use of the approximate HO_2 concentration given by (15), the water production rate can then be simplified as:

$$\frac{\mathrm{d}C_{\mathrm{H_2O}}}{\mathrm{d}t} = 2k_6 C_{\mathrm{HO}_2}^{*2}. \tag{28}$$

Since H_2 and O_2 have zero formation enthalpy, the heat released by the reactions mainly comes from the production of $\mathrm{H_2O}$, yielding

$$\frac{\mathrm{d}T}{\mathrm{d}t} = \frac{-2k_6 \Delta H^0_{\mathrm{H_2O}}}{\rho c_p} C_{\mathrm{HO}_2}^{*2}, \tag{29}$$

where ρ and c_p denote the fresh gas density and specific heat at constant pressure, while $\Delta H^0_{\mathrm{H_2O}}$ is the standard enthalpy of formation of gaseous $\mathrm{H_2O}$, equal to -241.8 kJ/mol.

In order to take into account the mechanism leading to the thermal runaway, the λ temperature dependence is required. Dimensionless activation energy β and temperature θ are introduced

$$\theta = \beta \frac{T - T_0}{T_0}, \tag{30}$$

with β to be explicited in Eq. (35). Assuming a single activation energy for λ in the low temperature range yields

$$\lambda(\theta) = \lambda e^{\theta}. \tag{31}$$

Following [15], the thermal runaway problem can then be expressed as :

$$\begin{cases} \dfrac{\mathrm{d}C_\eta}{\mathrm{d}t} = & C_\eta \lambda e^{\theta} \\ \dfrac{\mathrm{d}\theta}{\mathrm{d}t} = & qC_\eta^2, \end{cases} \tag{32}$$

with $q = \frac{-2k_6\beta\Delta H^0_{H_2O}}{T_0\rho c_p}$. Dividing the first equation to the second yields $\frac{\mathrm{d}\theta}{\mathrm{dC}_\eta} = \frac{qC_\eta}{\lambda e^\theta}$, which upon integration leads to

$$\theta(C_\eta) = \ln\left(1 + \frac{qC_\eta^2}{2\lambda}\right). \tag{33}$$

Using (33) and (31) finally lead to the modified reaction rate $\dot{\omega}_\eta$

$$\dot{\omega}_\eta = \left[\lambda^{(l_6)}C_\eta + \frac{q}{2}C^{*3}_{HO_2} + \epsilon_\eta\right] W_\eta. \tag{34}$$

Taking into account the thermal runaway can therefore be achieved by including a correcting cubic term in the scalar production rate below crossover. In this term, C_η has been conveniently replaced by $C^*_{HO_2}$, which is equal to C_η below crossover, but 0 above, where there is no thermal runaway. The above expression is therefore valid for all temperatures.

Expression (33) is fully explicit provided the dimensionless activation energy β. Given the complexity of λ, it was chosen to fit its dependence below crossover, where thermal runaway is important as

$$\beta = \frac{35038}{T} - 2.54, \tag{35}$$

yielding values slightly over 40 at 800K, more than enough for the high activation energy asymptotic analysis performed. In the system, reaction 8 is the most sensitive to temperature changes and 70% of the total increase of λ with temperature is related to this reaction, with a reduced activation energy close to 30 [15]. Figure 3.b presents the same ignition histories as Figure 3.a, now including the thermal runaway correction. Predictions are now excellent, showing that the present method is able to well reproduce ignition histories with a single scalar, e.g. without heat release.

A surprising result is that the present model allows for accurate prediction of the ignition histories below crossover without considering a temperature equation (thermal runaway would a priori require one). The reduced temperature can nonetheless be reconstructed accurately from Eq. (33) if needed. Such reconstruction corresponds to the superimposed dashed green line in Fig. 3.b, and displays an excellent agreement.

3.4. Passive scalar model validation

The overall capability of the new scalar model defined previously is assessed by comparing of the predicted ignition delays in perfectly stirred

reactors at constant pressure with those obtained by "exact" integration of the 8-step mechanism. Ignition delays computed with the previous scalar [13] are also reported to highlight the improvements below crossover.

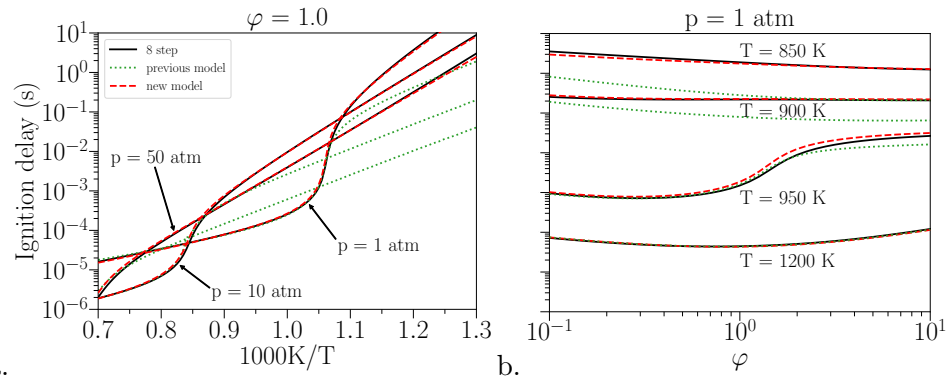

Figure 5: Comparison of ignition delays of an isobaric homogeneous ignition of an H_2-air mixture, obtained by numerical integration for the reduced 8-step chemistry (solid curves), the previous scalar model from [13] (green dotted curves) and the new scalar model (red dashed curve).

The ignition delays are compared in Figures 5.a and 5.b. Predicted ignition delays with the new scalar model exhibit an outstanding agreement with those computed with the chemistry of reference for the entire range of conditions in terms of temperature, pressure and equivalence ratio.

4. Description of the scalar diffusivity

Now that the scalar reaction rate has been revisited to be relevant for temperatures both below and above cross-over, a special attention needs to be taken to its diffusion properties. Indeed the main radicals present is those two regimes are completely different, and their diffusion properties as well. As a reminder, the radicals pool mainly consists of H at temperature higher that the cross-over temperature, which is 4 to 5 times more diffusive than HO_2 or H_2O_2 found for the low temperature regime.

4.1. Eigenvector based properties

Once the eigenvalue λ is obtained analytically, the associated eigenvector may also be obtained analytically:

$$\begin{cases} V_{\mathrm{H}} & = 1 \\ V_{\mathrm{O}} & = l_1 / \left(l_2 + \lambda\right) V_{\mathrm{H}} \\ V_{\mathrm{OH}} & = \left(l_1 V_{\mathrm{H}} + l_2 V_{\mathrm{O}} + 2 l_8 V_{\mathrm{H_2O_2}}\right) / \left(l_3 + \lambda\right) \\ V_{\mathrm{HO_2}} & = l_4 / \left(l_7 + 4 l_6 + \lambda\right) V_{\mathrm{H}} \\ V_{\mathrm{H_2O_2}} & = \left(l_7 + 2 l_6\right) / \left(l_8 + \lambda\right) V_{\mathrm{HO_2}}. \end{cases} \tag{36}$$

This analytically obtained eigenvector gives us information about the molar proportion of each radical in the radical pool, which is used to express Fig. 6. It can be used to model the diffusion coefficient of the scalar with a simple weighted average:

$$D_\eta = \sum_{k=1}^{5} D_k v_k, \tag{37}$$

with v_k the normalized eigenvector :

$$v_k = V_k / \sum_{k=1}^{5} V_k. \tag{38}$$

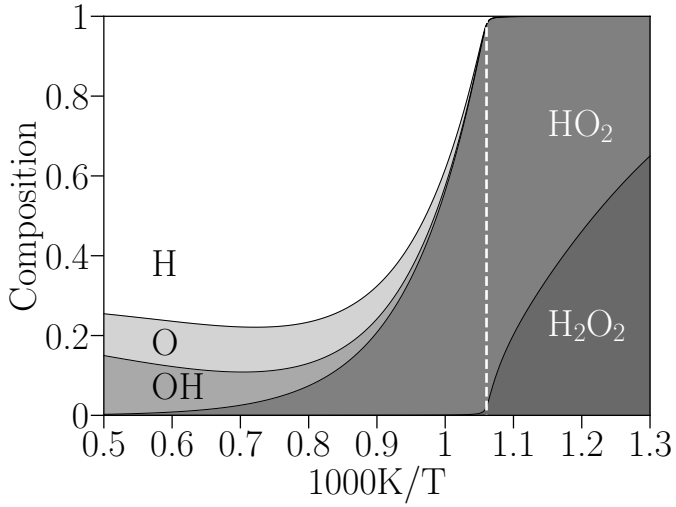

Figure 6: Radical-pool composition obtained from the normalized eigenvector associated with the dominant eigenvalue for p=1 atm, φ=1. The vertical line indicates the crossover.

Note that molar proportions are used for the weighted average to ensure consistency with the diffusion model used in Eq. (1) (as well as in most reactive flow solvers), which relies on the gradients of molar fractions.

This expression has the advantage of giving a diffusion coefficient that is both continuous (important for numerical stability) and representative of the radical pool. In order to highlight the importance of the diffusion properties of the scalar, a temporal mixing layer was simulated with the reduced chemistry and the new model for different choices of its diffusion coefficient. This simple configuration consists of a one-dimensional domain of 2 cm discretized in 500 points. The first half of the domain is initially filled with Air and the second part with a H_2-N_2 mixture (25% of H_2 in volume). The entire domain is initially set at a temperature of 1000 K and a pressure of 1 atmosphere. The simulations were performed using a hybrid Lattice Boltzmann solver, already presented in [13, 25–27].

Figure 7 reports the maximum concentrations of H, HO_2 and H_2O in the temporal mixing layer, to illustrate the importance of the choice of the diffusion coefficient. It is clear that a slowly diffusive carrier (HO_2) will lead to faster ignition (with a faster global rate), while the H-atom high diffusion significantly slows down the process. In this specific case, the auto-ignition time difference between the two extreme choices of diffusion coefficient is up to 13% of the ignition time obtained with the reduced chemistry. Using a weighted average of the main eigenvector for the scalar diffusion property seems good enough, providing an accurate ignition growth rate (and therefore an accurate delay).

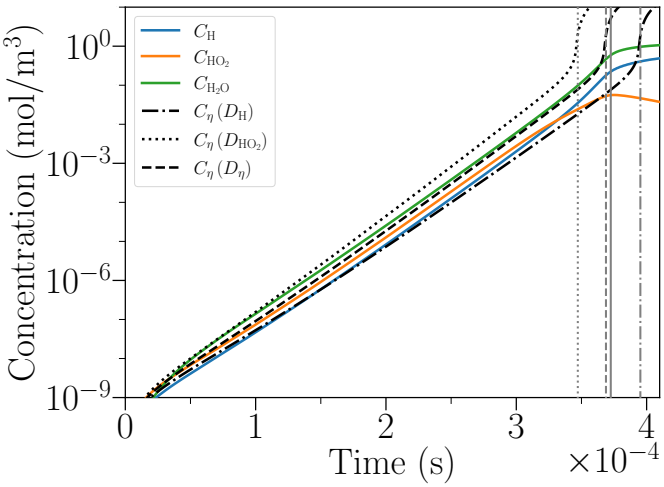

Figure 7: Evolution of the maximal concentration of the radicals in the domain for a temporal mixing layer (continuous curves). The evolution of the maximal value of the scalar is displayed (discontinuous black curves) for different diffusion coefficients used. Finally, the time of ignition is displayed (vertical grey lines) for each case.

Figure 8 presents the passive scalar profiles in the domain at a time $t = 3\times10^{-4}$ s. The profiles obtained using the diffusion coefficients of H, HO_2, or using Eq. (37) are compared to the scalar concentration reconstructed from the concentrations obtained from the reduced chemistry using the following relationships:

$$C_\eta = \bar{V}^L \bar{C} / \left(V^L_{\mathrm{H}} + V^L_{\mathrm{HO_2}}\right), \tag{39}$$

derived from A.1 for $\epsilon_\eta = \omega_5$.

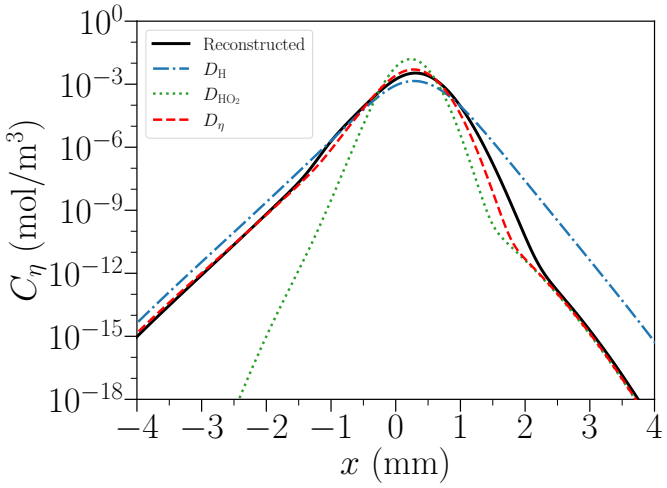

Figure 8: Comparison of the passive scalar concentration profiles for a temporally evolving mixing layer (one-dimensional) between the scalar reconstructed from the reduced chemistry results (solid curve), the scalar resulting from the use of diffusion coefficient of H (blue curve), of HO_2 (green curve), and using D_η (red curve).

It is clear that using a diffusion coefficient based on the composition (obtained with the eigenvectors) significantly improves the results. As expected, using the diffusion coefficient of a specific radical is only relevant in the region where that radical dominates, for example, in Fig. 8, H in the left part of the domain and HO_2 in the right part. However, even in those regions, the average value appears to provide a more representative diffusion process (as indicated by the over-estimation of the scalar concentration in the left part of the domain with D_{H}).

4.2. Turbulent mixing layer validation

Let us now assess the performance of the scalar model on a more challenging test case. A two-dimensional turbulent double mixing layer is adapted from [28] for high pressure. The domain is a 4.5 mm square discretized with 500×500 grid points. To form the double mixing layer, the first and last quarters of the domain along the x axis are initially filled with Air at 1200 K, and the remaining half of the domain is filled with a H_2-N_2 mixture (50-50 in volume) at 300 K. The pressure is set at 50 atmosphere pressure to be relevant for hydrogen storage. The velocity field is initialized to be weakly turbulent to emphasize the influence of the chemistry modeling. The turbulent field was generated using Rogallo's procedure [29] with a Passot-Pouquet spectrum [30]. A turbulent length scale of 0.45 mm and a root

mean square of the velocity fluctuations of 0.70 m/s were used, giving a turbulent time scale of 0.64 ms.

This configuration has been utilized to compare the growth of ignition kernels using different chemical models, including the San Diego mechanism, the reduced 8 step chemistry, the previous scalar model [13] (with the most relevant diffusion properties i.e. HO_2 for the present conditions) and finally the present updated scalar model with its average diffusion coefficient (37). The recorded time of the first ignition event is presented in Table 2, with the time step used, the reduced time to solution and a normalized computational cost index. The use of the updated scalar model is 43.7 times cheaper in terms of CPU cost compared to the full chemistry integration. Note that the four simulations have been performed using 20 cores on a dual CPU desktop (2 $\times$ Intel Xeon(R) Silver 4214R).

Table 2: Summary of the auto-ignition time τ_i, the time step Δt, the reduced time to solution RTTS (total CPU time in ms needed to simulate 1 ms for 1 cell) [31] and the cost (reduced time to solution with respect to the one of the scalar) of the four cases.

case	τ_i	Δt	RTTS	cost
San Diego	0.497 ms	3×10^{-9} s	1048	43.7
8 step	0.472 ms	1×10^{-8} s	218	9.1
Previous model with D_{HO_2}	0.826 ms	1×10^{-7} s	24	1.0
New model with D_η	0.464 ms	1×10^{-7} s	24	1.0

The temperature fields obtained for the reduced chemistry and the approximated one using equations (30) and (33) for the updated scalar model are shown Fig. 9 at 4 μs after the first ignition events. This qualitative comparison highlights the ability of the new scalar model to recover where ignition events occur.

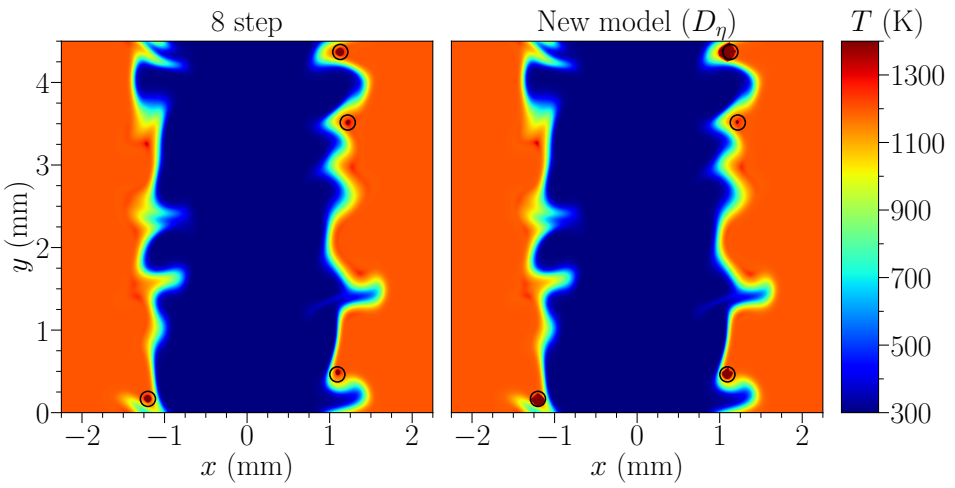

Figure 9: Comparison of the temperature fields obtained with the 8 step chemistry and with the new scalar model, taken 4 μs after the first ignition event. The four black circles identify the ignition kernels selected for Figure 10.

The temporal evolution of HO_2 concentrations are now reported at the four ignition kernels identified in Fig. 9 for quantitative validation between the detailed chemistry, 8-step chemistry, and the two scalar models. The new formulation of the scalar allows to recover precisely the ignition behavior of the reduced mechanism at a considerably lower cost, the difference between the new model and the detailed chemistry being mainly due to the slight discrepancies between the detailed and 8-step mechanisms. Expectingly, the previous scalar formulation [13] yields a strong overestimation of the ignition delays since it fails to consider the non-linearity of step 6 and thermal runaway.

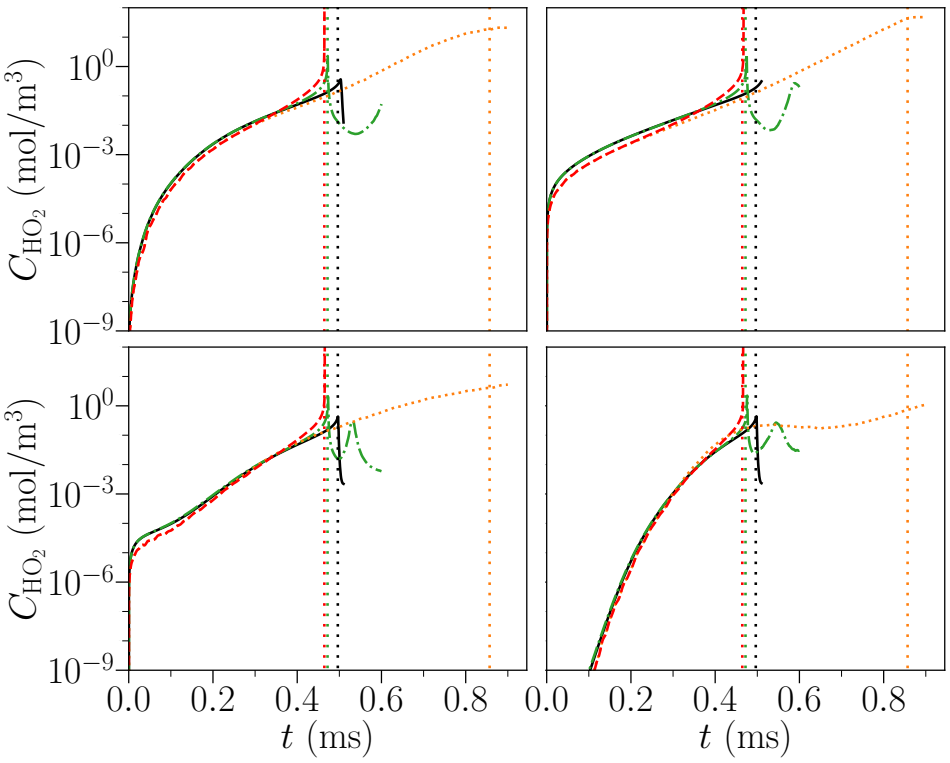

Figure 10: Evolution of the HO_2 concentrations at four positions of the mixing layer for reactive cases using the San Diego mechanism (black curve), the reduced 8 step (green dash-dotted curve), the previous scalar model (orange dotted curve) and the new scalar model (red dashed curve) using the averaged diffusion properties.

The scalar concentration profiles are also compared in Fig. 11. These profiles are obtained by sampling along the x direction across the first kernel to ignite (top right kernel) at a time of $t = 4.4 \times 10^{-4}$ s, which is close to ignition. For both the detailed and reduced chemistry models, the scalar is reconstructed using Eq. (39).

The new scalar model shows excellent agreement with the reduced chemistry, whereas the previous model fails to capture the correct profile in the highly reactive zone, particularly in terms of the kernel position. This discrepancy can be attributed to the incorrect reaction rate, as it misses the non-linear branching and thermal runaway phenomena, in addition to the oversimplified diffusion model, as previously demonstrated in Fig. 8. It also appears that the difference in chemistry between the detailed and reduced mechanisms primarily affects the ignition time of the kernel, while

the position of the kernel remains unchanged.

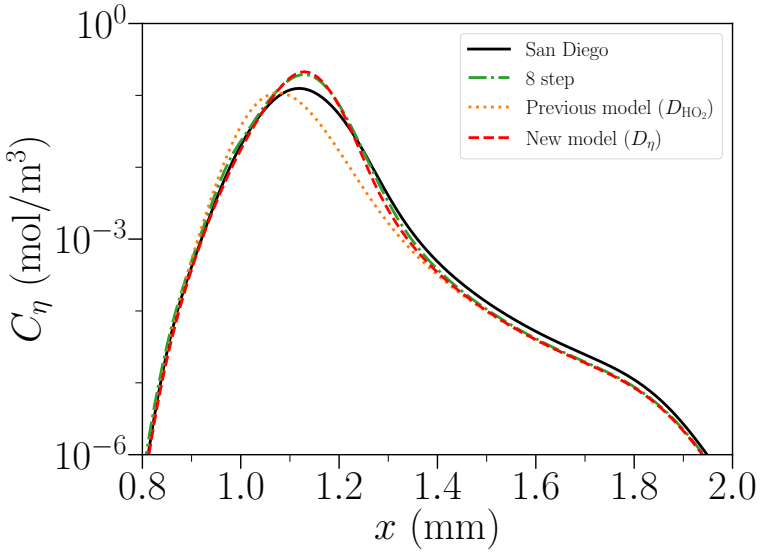

Figure 11: Comparison of the passive scalar concentration profiles along the x direction across the first kernel to ignite (top right) for the mixing layer at $t = 4.4 \times 10^{-4}$ s. Reconstructed scalar concentration from the San Diego mechanism (black curve), the reduced 8-step (green dash-dotted curve), the previous scalar model (orange dotted curve) and the new scalar model (red dashed curve) using the averaged diffusion properties.

5. Conclusion

We have presented a new passive scalar model able to predict ignition in complex flow configurations, building upon the scalar model presented by Taileb et al. [13], valid for temperatures above crossover.

The new formulation is still valid above crossover, but also in its vicinity, and the low-temperature limit. This is particularly useful for high-pressure configurations, ubiquitous in novel H_2 applications: the crossover temperature is 1430K at 50 bars (vs. 940K at 1 bar), putting most relevant ignition conditions below crossover.

Excellent accuracy is achieved by introducing three new elements to the model: (i) an extended formulation of the branching characteristic time λ taking into account the non-linear step $HO_2 + HO_2 \rightarrow H_2O_2 + O_2$ (step 6), (ii) a cubic correcting term to account for the thermal runaway, and (iii) a formulation for the scalar diffusivity which takes into account the radical pool composition, which may consist mainly of H-atom or HO_2 depending on local conditions.

The model is validated on homogeneous reactor configurations, 1D temporal mixing layers, and a 2D DNS double mixing layer. Future works will include safety analysis of more complex configurations.

6. Acknowlegments

Prof. Forman Williams is gratefully acknowledged for fruitful discussions on the scalar model formulation during summer of 2022. This research was supported by the MALBEC ANR project ANR-20-CE05-0009.

References

[1] B. Lewis, G. Von Elbe, Combustion, flames and explosions of gases, Elsevier, 2012.

[2] A. L. Sánchez, F. A. Williams, Recent advances in understanding of flammability characteristics of hydrogen, Prog. Energy Combust. Sci. 41 (2014) 1–55.

[3] A. L. Sánchez, E. Fernández-Tarrazo, P. Boivin, A. Liñán, F. A. Williams, Ignition time of hydrogen–air diffusion flames, Comptes Rendus Mecanique 340 (2012) 882–893.

[4] N. N. Semenov, Thermal theory of combustion and explosion, Progress of Physical Science 24 (NACA-TM-1026) (1942).

[5] D. A. Frank-Kamenetskii, Diffusion and heat exchange in chemical kinetics, Vol. 2171, Princeton University Press, 2015.

[6] H. W. Liepmann, A. Roshko, Elements of gasdynamics, Courier Corporation, 2001.

[7] E. F. Toro, Riemann solvers and numerical methods for fluid dynamics: a practical introduction, Springer Science & Business Media, 2013.

[8] V. Kurdyumov, J. Blasco, A. L. Sánchez Pérez, A. Liñán Martínez, On the calculation of the minimum ignition energy, Combust. Flame 136 (2004) 394–397.

[9] E. Fernández-Tarrazo, R. Gómez-Miguel, M. Sánchez-Sanz, Minimum ignition energy of hydrogen–ammonia blends in air, Fuel 337 (2023) 127128.

[10] J. Carpio, I. Iglesias, M. Vera, A. L. Sánchez, A. Liñán, Critical radius for hot-jet ignition of hydrogen–air mixtures, Int. J. Hydrog. Energy 38 (2013) 3105–3109.

[11] J. Carpio, I. Iglesias, M. Vera, A. L. Sánchez, Critical slot size for deflagration initiation by hot products discharge into hydrogen–air atmospheres, Int. J. Hydrog. Energy 42 (2017) 1298–1305.

[12] A. Millán-Merino, S. Taileb, P. Boivin, A new method for systematic 1-step chemistry reduction applied to hydrocarbon combustion, Proc. Combust. Inst. (2022). doi:https://doi.org/10.1016/j.proci.2022.08.052.

[13] S. Taileb, A. Millán-Merino, S. Zhao, P. Boivin, Lattice-boltzmann modeling of lifted hydrogen jet flames: A new model for hazardous ignition prediction, Combust. Flame 245 (2022) 112317.

[14] R. Cabra, T. Myhrvold, J. Chen, R. Dibble, A. Karpetis, R. Barlow, Simultaneous laser raman-rayleigh-lif measurements and numerical modeling results of a lifted turbulent H_2/N_2 jet flame in a vitiated coflow, Proc. Combust. Inst. 29 (2002) 1881–1888.

[15] P. Boivin, A. L. Sánchez, F. A. Williams, Explicit analytic prediction for hydrogen–oxygen ignition times at temperatures below crossover, Combust. Flame 159 (2012) 748–752.

[16] P. Boivin, A. Sánchez, F. Williams, Analytical prediction of syngas induction times, Combust. Flame 176 (2017) 489–499.

[17] P. Boivin, M. Le Boursicaud, A. Millan-Merino, S. Taileb, J. Melguizo-Gavilanes, F. A. Williams, Hydrogen ignition and safety, in: Hydrogen for future thermal engines, Springer, 2022.

[18] F. Williams, et al., Chemical-kinetic mechanisms for combustion applications, University of California, San Diego, version 2016-12-14, last accessed on 2023-02-22.
URL `http://web.eng.ucsd.edu/mae/groups/combustion/mechanism.html`

[19] C. Treviño, Ignition phenomena in h_2-o_2 mixtures, Progress in Astronautics and Aeronautics, AIAA 131 (1991) 19–43.

[20] G. Del Alamo, F. Williams, A. Sanchez, Hydrogen-oxygen induction times above crossover temperatures, Combust. Sci. Technol. 176 (2004) 1599–1626.

[21] A. L. Sánchez, E. Fernández-Tarrazo, F. A. Williams, The chemistry involved in the third explosion limit of H_2-O_2 mixtures, Combust. Flame 161 (2014) 111–117.

[22] P. Boivin, Reduced-kinetic mechanisms for hydrogen and syngas combustion including autoignition, Phd, Universidad Carlos III de Madrid (12 2011).

[23] W. Liang, C. K. Law, An analysis of the explosion limits of hydrogen/oxygen mixtures with nonlinear chain reactions, Phys. Chem. Chem. Phys. 20 (2018) 742–751.

[24] P. Boivin, C. Jiménez, A. Sánchez, F. Williams, An explicit reduced mechanism for H_2–air combustion, Proc. Combst. Inst. 33 (1) (2011) 517–523.

[25] M. Tayyab, S. Zhao, Y. Feng, P. Boivin, Hybrid regularized lattice-boltzmann modelling of premixed and non-premixed combustion processes, Combust. Flame 211 (2020) 173–184.

[26] G. Farag, T. Coratger, G. Wissocq, S. Zhao, P. Boivin, P. Sagaut, A unified hybrid lattice-boltzmann method for compressible flows: bridging between pressure-based and density-based methods, Phys. Fluids 33 (2021) 086101.

[27] G. Wang, S. Zhao, P. Boivin, E. Serre, P. Sagaut, A new hybrid lattice-boltzmann method for thermal flow simulations in low-mach number approximation, Phys. Fluids 34 (2022) 046114.

[28] H. G. Im, J. H. Chen, C. K. Law, Ignition of hydrogen-air mixing layer in turbulent flows, Symp. (Int.) Combust. 27 (1998) 1047–1056.

[29] R. S. Rogallo, Numerical experiments in homogeneous turbulence, Tech. Rep. NASA-TM-81315, NASA Ames Research Center (1981).

[30] T. Passot, A. Pouquet, Numerical simulation of compressible homogeneous flows in the turbulent regime, J. Fluid Mech. 181 (1987) 441–466.

[31] A. Abdelsamie, G. Lartigue, C. E. Frouzakis, D. Thévenin, The taylor–green vortex as a benchmark for high-fidelity combustion simulations using low-mach solvers, Comput. Fluids 223 (2021) 104935.

Appendix A. Derivation of ϵ_η

In order to highlight how to choose the value ϵ_η, let's rewrite the diagonalization of the Jacobian $\mathbf{A} = a\mathbf{P}\mathbf{D}\frac{1}{a}\mathbf{P}^{-1}$ with a the coefficient representing the dimension one of the eigenvectors. The scalar is then defined as

$$C_\eta = \frac{1}{a}\bar{V}^L\bar{C}, \tag{A.1}$$

and its initial reaction rate reads:

$$\epsilon_\eta = \omega_5 \left(V^L_{\mathrm{H}} + V^L_{\mathrm{HO_2}}\right)/a. \tag{A.2}$$

Eq. (A.1) can be rewritten as (by definition of the left and right eigenvector, $\bar{V}^R\bar{V}^L = 1$):

$$\bar{C} = a\bar{V}^R C_\eta, \tag{A.3}$$

this relationship can be used to enforce an expression for a that will be used in (A.2) to define precisely ϵ_η. As it is discussed in Section 3.1, we intend to set $C_\eta = C_{\mathrm{HO_2}}$ below the cross-over, meaning that:

$$a = 1/V^R_{\mathrm{HO_2}}, \tag{A.4}$$

leading the initial reaction rate to be:

$$\epsilon_\eta = \omega_5 \left(V^L_{\mathrm{H}} + V^L_{\mathrm{HO_2}}\right) V^R_{\mathrm{HO_2}}. \tag{A.5}$$

The difficulty lies in obtaining the left eigenvector $\bar{V}^L$, and a simpler approximation such as:

$$\epsilon_\eta = \omega_5 \tag{A.6}$$

has been retained, and corresponds to:

$$a = V^L_{\mathrm{H}} + V^L_{\mathrm{HO_2}}. \tag{A.7}$$

This leads to the following relationship between the scalar and the radicals concentration :

$$C_k/C_\eta = V^R_k \left(V^L_{\mathrm{H}} + V^L_{\mathrm{HO_2}}\right). \tag{A.8}$$

The ratio $C_{\mathrm{HO_2}}/C_\eta$ obtained numerically is plotted in Figure A.12 for a large range of temperature and pressure in the case of the simplification (A.6). The ratio is indeed close to unity for low temperature, however the real concentration is as much as 20 times larger that the approximate value

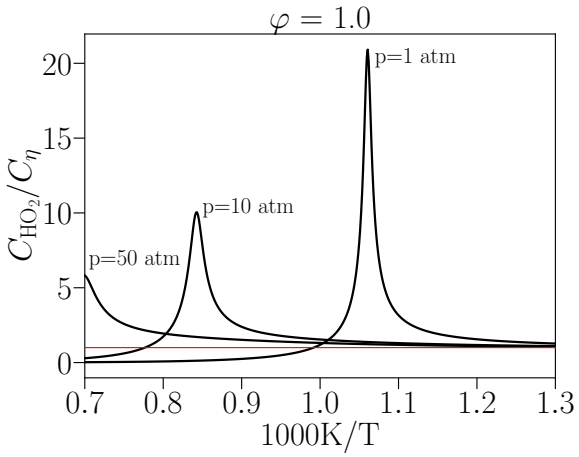

Figure A.12: Evolution of the theoretical ratio between the HO_2 and the scalar concentrations (black) in the case of the simplification (A.6), for a stoichiometric hydrogen-air mixture. The unity ratio is highlighted with the red line.

close at the cross-over. Fortunately, the estimation of the HO_2 concentration is only needed when the non-linear reaction 6 is no more negligible below the cross-over.

The impact of this simplification on the ignition delay is investigated hereafter for large range of temperature and pressure. Figure A.13.a displays the ignition delays obtained by integration of Eq. 33 with the exact expression (A.5), while Figure A.13.b shows the result obtained with the approximation (A.6). Both expressions give an excellent agreement with the ignition delay obtained from the 8-step mechanism. The small differences obtained close to crossover (almost imperceptible) were found irrelevant, since errors between the 8-step and detailed description (Fig. 1) – or even from a detailed mechanism to another – are much more pronounced.

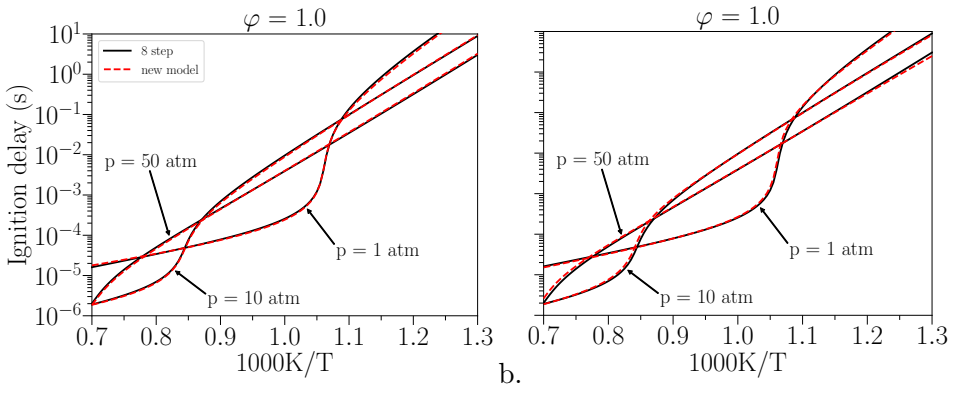

Figure A.13: Comparison of ignition delays of an isobaric homogeneous ignition of an H_2-air mixture, obtained by numerical integration for the reduced 8-step chemistry (solid curves) and the new model (red dashed curve). The left figure use formula (A.5) with $C^*_{HO_2} = C_\eta$ while the right figure use the simplified version (A.6) along with the relationship (15).

The simplified expression $\epsilon_\eta = \omega_5$ has therefore been retained for simplicity, throughout this study.

Appendix B. Choice of W_η

Eq. (1) make appear W_η trough Eq. (10), we choose to model it as a constant. By doing so C_η becomes completely independent of the value uses for W_η. Indeed, making use of the relation $\rho\eta = W_\eta C_\eta$, Eq. (1) can be rewritten as :

$$\frac{\partial W_\eta C_\eta}{\partial t} + \frac{\partial u_\alpha W_\eta C_\eta}{\partial x_\alpha} = \frac{\partial}{\partial x_\alpha}\left(\rho D_\eta \frac{W_\eta}{W}\frac{\partial}{\partial x_\alpha}\left(\frac{W}{\rho}C_\eta\right)\right) + W_\eta\left(\lambda C_\eta + \epsilon_\eta\right). \tag{B.1}$$

Since W_η is a constant, it can be taken out of the derivatives and simplified to give the transport equation of C_η :

$$\frac{\partial C_\eta}{\partial t} + \frac{\partial u_\alpha C_\eta}{\partial x_\alpha} = \frac{\partial}{\partial x_\alpha}\left(\frac{\rho D_\eta}{W}\frac{\partial}{\partial x_\alpha}\left(\frac{W}{\rho}C_\eta\right)\right) + \left(\lambda C_\eta + \epsilon_\eta\right). \tag{B.2}$$

C_η and so the ignition prediction is independent of W_η, which only appears to transport the scalar with a classical mass fraction transport equation and does not impact the results.

Appendix C. Analytical solution for the 3×3 matrix largest real eigenvalue

Finding the eigenvalues of a matrix is equivalent to finding the zeros of its characteristic polynomial. In the case of a 3×3 matrix, its characteristic polynomial is of the third order and can be written as:

$$\lambda^3 + a_2\lambda^2 + a_1\lambda + a_0 = 0 \tag{C.1}$$

Using the Cardan method to find the root of the polynomial (C.1), a new variable is defined $z = \lambda + a_2/3$ and leads to finding the root of this new polynomial:

$$z^3 + pz + q = 0 \tag{C.2}$$

with

$$\begin{cases} p &= a_1 - a_2^2/3 \\ q &= a_0 + 2a_2^3/27 - a_1a_2/3. \end{cases} \tag{C.3}$$

The discriminant is expressed as $\Delta = -(4p^3 + 27q^2)$, the largest root will be found with a different formula depending of the discriminant sign.

If $\Delta < 0$, there is only one real root, to simplify the formula, we define $\delta = \sqrt{-\Delta/27}$ to express the root as:

$$z_0 = \sqrt[3]{\frac{-q+\delta}{2}} + \sqrt[3]{\frac{-q-\delta}{2}}. \tag{C.4}$$

If $\Delta > 0$ ($p < 0$ necessarily then), there is three real roots and the largest of them reads:

$$z_0 = 2\sqrt{\frac{-p}{3}}\cos\left(\frac{\arccos\left(\frac{3q}{2p}\sqrt{\frac{-3}{p}}\right)}{3}\right). \tag{C.5}$$

If $\Delta = 0$, there is two real roots, a single ($3q/p$) and a double one ($-3q/2p$) (its a triple root if $p = q = 0$).

In the end, the largest eigenvalue of the 3×3 matrix reads:

$$\lambda = \begin{cases} \sqrt[3]{\frac{-q+\delta}{2}} + \sqrt[3]{\frac{-q-\delta}{2}} - \frac{a_2}{3} & \text{if } \Delta < 0 \\ \max\left(\frac{3q}{p}, -\frac{3q}{2p}\right) - \frac{a_2}{3} & \text{if } \Delta = 0 \\ 2\sqrt{\frac{-p}{3}}\cos\left(\frac{\arccos\left(\frac{3q}{2p}\sqrt{\frac{-3}{p}}\right)}{3}\right) - \frac{a_2}{3} & \text{if } \Delta > 0 \end{cases} \tag{C.6}$$